

# Anisotropy probe of galactic and extra-galactic Dark Matter annihilations

Mattia Fornasa\*

*University of Padova & INFN sezione di Padova, via Marzolo 8, 35131 Padova, Italy and  
Institut d'Astrophysique de Paris, boulevard Arago 89bis, 75014 Paris, France*

Lidia Pieri<sup>†</sup> and Gianfranco Bertone<sup>‡</sup>

*Institut d'Astrophysique de Paris, UMR 7095-CNRS,  
Université Pierre et Marie Curie, boulevard Arago 89bis, 75014 Paris, France*

Enzo Branchini<sup>§</sup>

*Department of Physics, Università di Roma Tre, via della Vasca Navale 84, 00146, Rome, Italy*

We study the flux and the angular power spectrum of gamma-rays produced by Dark Matter annihilations in the Milky Way (MW) and in extra-galactic halos. The annihilation signal receives contributions from: a) the smooth MW halo, b) resolved and unresolved substructures in the MW, c) external DM halos at all redshifts, including d) their substructures. Adopting a self-consistent description of local and extra-galactic substructures, we show that the annihilation flux from substructures in the MW dominates over all the other components for angles larger than  $\mathcal{O}(1)$  degrees from the Galactic Center, unless an extreme prescription is adopted for the substructures concentration. We also compute the angular power spectrum of gamma-ray anisotropies and find that, for an optimistic choice of the particle physics parameters, an interesting signature of DM annihilations could soon be discovered by the Fermi LAT satellite at low multipoles,  $\ell \lesssim 100$ , where the dominant contribution comes from MW substructures with mass  $M \gtrsim 10^4 M_\odot$ . For the substructures models we have adopted, we find that the contribution of extra-galactic annihilations is instead negligible at all scales.

PACS numbers:

## I. INTRODUCTION

Despite the compelling evidence for Dark Matter (DM), we know very little about its nature. It is commonly assumed that DM is composed of Weakly Interacting Massive Particles (WIMPs), that are kept in thermal and kinetic equilibrium with baryons in the early universe through their weak coupling with ordinary matter, and that subsequently decouple from them when the self-annihilation rate drops below the expansion rate of the universe, thus naturally achieving the appropriate relic density. Being proportional to the square of the DM number density, the self-annihilation rate is today very small, but it can still lead to detectable signals in regions with very high DM density [1, 2].

Indirect DM searches are based on the detection of particles originating from DM annihilation or decay. If one focuses on the most widely discussed candidates, i.e. the supersymmetric neutralino and the so-called  $B^{(1)}$  in theories with Universal Extra Dimensions, the mass of the DM particles should be approximately in the 100 GeV – 1 TeV range, and the characteristic energy of the produced particles, roughly an order of magnitude smaller. At these energies, photons are among the best messen-

gers, since gamma-rays travel in the local universe along geodesics without significant energy losses.

The most obvious target for indirect DM searches is the center of our Galaxy, where the large concentration of ordinary matter is believed to be associated to a large DM density enhancement. However, the search for gamma-rays from DM annihilations in the Galactic Center (GC) is complicated by the presence of a strong signal of astrophysical origin, due to the point sources detected by the EGRET satellite [3, 4, 5] and by the H.E.S.S. telescope [6]. A further degree of complication is constituted by theoretical uncertainties on the DM profile in the innermost regions of the MW halo which is inevitably affected by the presence of a SuperMassive Black Hole and by the surrounding distribution of stars [7, 8].

To avoid such difficulties, different authors have suggested alternative strategies to unambiguously detect the signature of DM interpretation. One possibility is to look for enhancements in the gamma-ray flux with no obvious astrophysical origin. Moreover, the presence of possible distinctive features in the gamma-ray energy spectrum (as lines [9, 10] or “bumps” [11]) may help in ruling out alternative, more conventional, interpretations. Ando et al. [12, 13] have recently pointed out that unique annihilation features may also be detected in the angular correlation properties of the Extragalactic Gamma-ray Background (EGB). From an observational point of view the EGB is obtained by subtracting the galactic gamma-ray flux produced by cosmic-rays interacting with the interstellar medium at high galactic latitude from the to-

---

\*Electronic address: mfornasa@pd.infn.it

†Electronic address: pieri@iap.fr

‡Electronic address: bertone@iap.fr

§Electronic address: branchin@fis.uniroma3.it

tal background measured by EGRET [14]. The resulting EGB is isotropic and its energy spectrum is rather uncertain, especially at energies above 10 GeV [15, 16, 17]. Unresolved extra-galactic gamma-ray sources like blazars certainly contribute to the EGB. However, current uncertainties on the luminosity function of these objects do not allow to exclude additional contributions from more exotic processes like DM annihilation within and outside our Galaxy.

The annihilation signal along a given direction in the sky is contributed by four different sources:

- the smooth MW halo, that is expected to contribute most towards the GC where the DM density enhancement is expected to be very large (see references above),
- resolved and unresolved substructures within the MW halo (see [18] and references therein).
- extra-galactic DM halos at all redshifts [19], including
- their substructures.

Ando et al. have shown that if DM annihilations in extra-galactic halos and their substructures contribute more than 30% to the EGB, the recently launched Fermi LAT satellite should be able to identify this 'exotic' contribution in the angular power spectrum.

Their analysis does not account for the possible contribution of galactic substructures to the angular correlation signal [12, 13]. Such contribution has been studied recently by Siegal-Gaskins who concluded that detectable features in the EGB angular power spectrum may exist and they can be used to infer the presence of galactic substructures and constrain their abundance [21] (in this case, annihilations in extra-galactic halos have been neglected).

Our model for galactic substructures is taken from Ref. [18], which is inspired by the high resolution N-body simulations aimed, precisely, at resolving subclumps within galaxy-sized halos (see Refs. [24, 28] and the more recent Refs. [30, 31, 32]). At  $z = 0$ , substructures are predicted to span 12 orders of magnitude in mass. Thus, the description of smaller objects is based on the extrapolation from the results at higher masses, since resolving such small clumps would be well beyond the resolution limit of the N-body experiments. In the attempt of limiting the theoretical uncertainties involved in this extrapolation, we have adopted two different prescriptions for the concentration of DM halos and subhalos of mass  $M$  as a function of redshift  $z$ ,  $c(M, z)$ . Then, to compute the gamma-ray fluxes from the resulting  $\sim 10^{16}$  galactic substructures, we have used the hybrid analytical and Monte Carlo approach described in Ref. [18].

The extra-galactic flux has been modeled using the formalism of Ref. [19], adapted to our calculation setup. In this way, we were able to compute for the first time in

a self-consistent way the normalization of the DM extra-galactic signal relative to the DM galactic foreground, a quantity that does *not* depend explicitly on the particle physics parameters (a weak implicit dependence remains, since the lower limit of integration of the subhalo mass function is sensitive to the particular particle physics scenario).

We have then computed the angular power spectra by running the public code **HEALPix** on our mock maps of galactic substructures, and comparing our result to those of Ref. [13] and Ref. [21].

The paper is organized as follows: in Sections II-IV we describe the theoretical setup, the properties of our model substructures and compute the mock full-sky maps of the gamma-ray flux due to DM annihilations, both galactic and extra-galactic. In Section V we compute the angular power spectrum of the mock gamma-ray sky and simulate its measurement using Fermi LAT in Section VI. Finally, in Section VII we draw our main conclusions and discuss our results.

## II. SIMULATION OF GALACTIC SUBSTRUCTURES

The Cold Dark Matter scenario predicts the formation of a large number of DM halos, virialized structures with masses possibly as small as  $\sim 10^{-6} M_{\odot}$  [22, 23]. Such halos merge into larger and larger systems, leading to the formation of today's halos of galaxies and clusters of galaxies. A fraction of the small halos survives to dynamical interactions with the stellar and dark components until the present epoch. Earth-size substructures have indeed been found in numerical simulations within DM halos of mass  $\sim 0.1 M_{\odot}$  at a redshift of 74 [24].

Resolving such small structures within a galaxy-sized halo today is out of computational reach, so that their spatial distribution, mass function and internal structure can only be estimated upon a rather uncertain extrapolation from the properties of higher mass satellites. Here, we work under the following hypotheses:

- we assume that substructures trace the mass of the MW, i.e that their radial distribution follows the mass density profile of the parent halo (as found e.g. in Ref. [24], see however the discussion below on the results of the most recent numerical simulations),
- we assume that the substructures mass function is well approximated by a power-law  $dn(M)/d\ln(M) \propto M^{-1}$ , normalized so that 10% of the MW mass lies in objects within the mass range  $10^{-5} M_{\text{MW}} - 10^{-2} M_{\text{MW}}$ , as found in Ref. [25].

Under these assumptions, the number density of subhalos per unit mass at a distance  $R$  from the GC can be

written as:

$$\rho_{sh}(M, R) = AM^{-2} \frac{\theta(R - r_{min}(M))}{(R/r_s^{MW})(1 + R/r_s^{MW})^2} M_\odot^{-1} \text{kpc}^{-3}, \quad (1)$$

where  $r_s^{MW}$  is the scale radius of our Galaxy and the effect of tidal disruption is accounted for by the Heaviside step function  $\theta(R - r_{min}(M))$ . The tidal radius,  $r_{min}(M)$ , is found by using the Roche criterion to decide whether a subhalo of mass  $M$  survives tidal interaction with the host halo (see Ref. [18]). According to our normalization about 53% of the MW mass is condensed within  $\sim 1.5 \times 10^{16}$  subhalos with masses in the range  $10^{-6} - 10^{10} M_\odot$ . Their abundance in the solar neighborhood turns out to be  $\sim 100$  subhalos  $\text{pc}^{-3}$ .

As far as the smooth component of the Galactic halo is concerned, we assume that the MW halo follows a Navarro, Frenk & White (NFW) profile [26, 27], with a scale radius  $r_s^{MW} = 21.7 \text{kpc}$  and that the total mass enclosed in a radius  $r_{200}$ , corresponding to the radius where the halo density is 200 times the critical density of the universe, is  $M_{MW} = 10^{12} M_\odot$ . An NFW fit to the DM halo of our Galaxy is consistent within 10% with the results of the *Via Lactea I* simulation [28]. A popular way to characterize the mass distribution within the DM halo is using the so-called *concentration*, a shape parameter defined as the ratio between the virial radius and the scale radius,  $c \equiv r_{200}/r_s$ .

Subhalos are also assumed to follow an NFW profile, with a concentration that depends on their mass [24]. To determine the dependence of concentration on the mass, we follow the prescription proposed in Ref. [29] (hereafter B01) in which the concentration parameter is found to depend on both the subhalo mass  $M_h$  and on its collapse redshift,  $z_c$ , defined as the epoch in which a mass scale  $M_h$  enters the non-linear regime. The collapse occurs when  $\sigma(M_h)D(z_c) \sim 1$ , where  $\sigma(M_h)$  is the present linear theory amplitude of mass fluctuations on the scale  $M_h$  and  $D(z_c)$  is the linear theory growth factor at the redshift  $z_c$ . In an attempt to bracket our theoretical uncertainties in modeling  $c(M_h, z_c)$  and its extrapolation at low masses we have implemented two rather extreme models chosen among those considered in Ref. [18], namely:

- $B_{z_0,ref}$ : that extrapolates the  $c(M_h, z_c)$  relation of B01 below  $10^4 M_\odot$  with a simple power-law,
- $B_{z_f,ref}$ : which assumes that surviving subhalos do not change their density profile since their formation. Thus the concentration parameter at  $z_c$  can be obtained from the one at  $z = 0$  through  $c(M_h, z_c) = c(M_h, z = 0)/(1 + z_c)$ . The values of  $c(M_h, z = 0)$  corresponds to those of the  $B_{z_0,ref}$  case and the collapse redshift  $z_c$  is obtained by extrapolating the expression proposed by B01 below  $10^4 M_\odot$ .

Finally, the concentration parameters are not uniquely defined by the halo mass. Rather, they follow a log-

normal distribution with dispersion  $\sigma_c = 0.24$  [29] and mean  $\bar{c}(M)$ :

$$P(\bar{c}(M), c) = \frac{1}{\sqrt{2\pi}\sigma_c c} e^{-\left(\frac{\ln(c) - \ln(\bar{c}(M))}{\sqrt{2}\sigma_c}\right)^2}. \quad (2)$$

### A. Recent highlights from numerical simulations

Two new sets of very high resolution numerical experiments have been recently released, namely the *Via Lactea II* [30] and the *Aquarius* [31, 32] simulations. The main characteristics of the MW subhalo population in these two simulations are summarized in Table I and compared to those of our subhalos. Among the main differences, we note that the mass fraction in substructures is a factor 2-6 smaller than that used in our model. Another difference is in the subhalo distribution which, in our case, trace the smooth mass distribution of the MW halo,  $\rho_{MW}(r)$ , while Refs. [31, 32] suggest to use an Einasto profile [33] and in *Via Lactea II* the innermost regions are best fitted by a power-law  $(1 + r)^{-2}$ .

The concentration parameter of subhalos in the two simulations depends from the distance from the GC and, in the *Aquarius* case, follows the prescription in Ref. [34] (N07) rather than the B01 model. Finally, in *Aquarius*, the subhalo density profile is also parametrized as an Einasto, rather than an NFW, profile.

These differences, in particular the fact that neither in *Via Lactea II* nor in *Aquarius* the spatial distribution of subhalos trace the mass of the parent halo, do have a significant impact on the angular power spectrum of the gamma-ray flux, as we will show in an upcoming publication. Here, we perform all calculations under the assumptions listed above, and discuss how the differences among the subhalo models in Table I are expected to affect the angular power spectrum (Section VII).

## III. MODELING THE GAMMA-RAY FLUX

### A. Gamma-ray flux from galactic subhalos

The gamma-ray flux expected from the annihilation of DM particles can be written as:

$$\frac{d\Phi_\gamma}{dE_\gamma}(E_\gamma, l, b) = \frac{d\Phi_\gamma^{PP}}{dE_\gamma}(E_\gamma) \times \Phi^{\text{cosmo}}(l, b) \quad (3)$$

where the term

$$\frac{d\Phi_\gamma^{PP}}{dE_\gamma}(E_\gamma) = \frac{1}{4\pi} \frac{\sigma_{\text{ann}} v}{2m_\chi^2} \cdot \sum_f \frac{dN_\gamma^f}{dE_\gamma} B_f \quad (4)$$

contains the dependence on particle physics parameters, while

$$\Phi^{\text{cosmo}}(\psi, l, b) = \int_M dM \int_c dc \int \int_{\Delta\Omega} d\theta d\phi \int_{\text{l.o.s}} d\lambda$$

|                            | this paper           | <i>Aquarius</i>                      | <i>Via Lactea II</i> |
|----------------------------|----------------------|--------------------------------------|----------------------|
| clumpiness ( $< r_{200}$ ) | 53%                  | 8%                                   | 26%                  |
| $N_{subhalos}(< r_{200})$  | $1.5 \times 10^{16}$ | $2.3 \times 10^{14}$                 | $7 \times 10^{15}$   |
| $dn/dM$                    | $\propto M^{-2}$     | $\propto M^{-1.9}$                   | $\propto M^{-2}$     |
| $n_{sh}(R)$                | NFW                  | Einasto<br>$\alpha_{Einasto} = 0.68$ | $\propto (1+R)^{-2}$ |
| $c(M, z)$                  | B01                  | N07                                  | B01                  |
| $\rho_{MW}(r)$             | NFW                  | Einasto<br>$\alpha_{Einasto} = 0.21$ | NFW                  |
| $\rho_{halo}(R)$           | NFW                  | Einasto<br>$\alpha_{Einasto} = 0.16$ | NFW                  |

TABLE I: The main characteristics of the subhalo model considered in this work compared with those measured in the recent *Aquarius* and *Via Lactea II* N-body simulations. The clumpiness is defined as the fraction of the dark mass in substructures within the virial radius of the MW  $r_{200} = 210$  kpc.  $N_{subhalos}$  is the total number of substructures within  $r_{200}$ .  $dn/dM$  is the subhalo mass function,  $n_{sh}(r)$  their radial distribution and  $c(M, z)$  is the model used for the concentration.  $\rho_{MW}$  and  $\rho_{halo}$  represent the mass density profile of the host halo and its substructures, respectively.

$$[\rho_{sh}(M, R(R_{\odot}, \lambda, l, b, \theta, \phi)) \times P(c) \times \Phi_{halo}^{\text{cosmo}}(M, c, r(\lambda, l, b, \theta, \phi)) \times J(x, y, z|\lambda, \theta, \phi)] \quad (5)$$

represents the contribution to the foreground emission from the subhalo population and

$$\Phi_{halo}^{\text{cosmo}}(M, c, r) = \int \int_{\Delta\Omega} d\phi' d\theta' \int_{1.o.s} d\lambda' \left[ \frac{\rho_{halo}^2(M, c, r(\lambda, \lambda', l, b, \theta', \phi'))}{\lambda^2} J(x, y, z|\lambda', \theta', \phi') \right] \quad (6)$$

is the contribution from a single subhalo.

The total galactic flux is obtained by adding to Eq. 5 the contribution of DM annihilations in the smooth NFW halo of the MW.

In Eq. 4,  $m_{\chi}$  is the DM particle mass,  $\sigma_{\text{ann}}v$  the annihilation cross section, and  $dN_{\gamma}^f/dE_{\gamma}$  the differential photon spectrum per annihilation relative to the final state  $f$ , with branching ratio  $B_f$  that we take from Ref. [35]. In this work we adopt a rather optimistic particle physics scenario (in the sense that it provides large annihilation fluxes), in which the DM particle has a mass  $m_{\chi} = 40$  GeV, a cross section  $\sigma v = 3 \times 10^{-26} \text{cm}^3 \text{s}^{-1}$  and particles annihilate entirely in  $b\bar{b}$ .

In Eq. 5,  $\Delta\Omega = 9.57 \times 10^{-6} \text{sr}$  is the solid angle considered for the integration, corresponding to the angular resolution of the Fermi LAT satellite,  $(l, b)$  are the galactic coordinates of the direction of observation, and  $J$  is the Jacobian determinant of the transformation between polar and cartesian coordinate systems. The galactocentric

distance,  $R$ , can be written as a function of the coordinates inside the observation cone  $(\lambda, \theta, \phi)$  and of  $(l, b)$  through the relation  $R = \sqrt{\lambda^2 + R_{\odot}^2 - 2\lambda R_{\odot} C}$ , where  $R_{\odot}$  is the distance of the earth from the GC, and  $C$  is the cosine of the angle between the direction of observation and the direction of the GC.

## B. Gamma-ray flux from extra-galactic structures

Aside from local DM, the gamma-ray flux in any given direction receives a contribution from all the structures at all redshift along the line of sight. Adapting the formalism of Ref. [19], we estimate here the contribution of extra-galactic structures, including the presence of substructures following the  $B_{z_0,ref}$  and  $B_{z_f,ref}$  models.

Following Ref. [19], the infinitesimal volume  $dV$  at a redshift  $z$  can be written as

$$dV = \frac{R_0^3 r^2 dr d\Omega}{(1+z)^3}, \quad (7)$$

where  $d\Omega$  is the solid angle,  $dr$  is the infinitesimal comoving depth and  $R_0$  is the scale factor at the present epoch. If, for a moment, we neglect the presence of subhalos and assume that the gamma-ray emission is isotropic, we can compute the number  $dN_{\gamma}$  of gamma-ray photons produced in  $dV$  in a time interval  $dt$  with an energy between  $E$  and  $E + dE$  and collected by a detector with effective area  $dA$  by integrating the single halo emissivity over the halo mass function  $\frac{dn}{dM}(M, z)$ :

$$dN_{\gamma} = e^{-\tau(z, E_0)} \left[ (1+z)^3 \int dM \frac{dn}{dM}(M, z) \frac{dN_{\gamma}}{dE}(E, M, z) \frac{dV dA}{4\pi R_0^2 r^2} dE_0 dt_0 \right], \quad (8)$$

where  $E_0$  and  $dt_0$  are, respectively, the energy and the time interval over which the photons are detected on earth. These quantities are related to those at the redshift of emission through  $E_0 = E/(1+z)$  and  $dt_0 = (1+z)dt$ , so that  $dt_0 dE_0 = dt dE$ . The halo mass function,  $dn/dM$ , represents the comoving number density of DM halos of mass  $M$  at redshift  $z$  and the factor  $(1+z)^3$  converts comoving into physical volumes. In the Press-Schechter formalism [36], the halo mass function is

$$\frac{dn}{dM}(M, z) = \frac{\rho_{\text{cr}} \Omega_{0,m}}{M^2} \nu f(\nu) \frac{d \log \nu}{d \log M}, \quad (9)$$

where  $\rho_{\text{cr}}$  is the critical density,  $\Omega_{0,m}$  is the mass density parameter,  $\nu = \frac{\delta_{sc}(z)}{\sigma(M)}$ ,  $\sigma(M)$  is the rms density fluctuation on the mass scale  $M$  and  $\delta_{sc}$  represents the critical density for spherical collapse. We refer to Refs. [19], [37] and [38] for the exact computation of these quantities.

$dN_{\gamma}/dE$  represents the number of photons with energy between  $E$  and  $E + dE$  produced in a halo of mass  $M$  at redshift  $z$ . The exponential  $e^{-\tau(z, E_0)}$  is an absorption coefficient that accounts for pair production due

to the interaction of the gamma-ray photons with the extra-galactic background light in the optical and infrared bands. Following Ref. [20], we adopt here the following expression that accounts for current observational constraints:  $\tau(z, E_0) = z/[3.3(E_0/10 \text{ GeV})^{-0.8}]$ . The mean flux is obtained by integrating Eq. 8 along the line-of-sight:

$$\begin{aligned} & \left\langle \frac{d\Phi}{dE_0 d\Omega} \right\rangle (E_0) \equiv \frac{dN_\gamma}{dE_0 dt_0 dAd\Omega} \quad (10) \\ &= \frac{1}{4\pi} \int dr R_0 e^{-\tau(z, E_0)} \\ & \int dM \frac{dn}{dM}(M, z) \frac{dN_\gamma}{dE}(E_0(1+z), M, z) \\ &= \frac{c}{4\pi} \int dz \frac{e^{-\tau(z, E_0)}}{H_0 h(z)} \\ & \int dM \frac{dn}{dM}(M, z) \frac{dN_\gamma}{dE}(E_0(1+z), M, z), \end{aligned}$$

where the last expression has been obtained by transforming comoving distances  $r$  into redshifts  $z$ , through the introduction of the Hubble parameter  $H_0 h(z) = H_0 \sqrt{\Omega_{0,m}(1+z)^3 + \Omega_{0,\Lambda}}$ , where  $H_0$  is the Hubble constant and  $\Omega_{0,i}$  the abundance in units of the critical density at  $z = 0$ .

The number of photons emitted in a single halo,  $dN_\gamma/dE$ , depends on the DM density profile (NFW in our case) and on the particle physics scenario (particle mass  $m_\chi$ , annihilation cross section  $\sigma v$  and differential energy spectrum per annihilation,  $dN_\gamma/dE_0$ ). The NFW profile of a halo with mass  $M$  is completely specified by the concentration parameter and the virial overdensity  $\Delta_{vir}$  of the halo. The virial radius  $r_{vir}$ , as opposed to the previously defined  $r_{200}$ , is the radius of the sphere which enclosed an average density  $\Delta_{vir} \times \rho_m$ . To be consistent with the notation used in Ref. [19] we define the concentration parameter as  $c(M, z) = r_{vir}/r_s$  and change the corresponding values in models  $B_{z_0, ref}$  and  $B_{z_f, ref}$  accordingly.

Bearing all this in mind, we can express  $dN_\gamma/dE$  as

$$\begin{aligned} \frac{dN_\gamma}{dE}(E, M, z) &= \frac{\sigma v}{2} \frac{dN_\gamma(E)}{E} \frac{M}{m_\chi^2} \frac{\Delta_{vir} \rho_{cr} \Omega_m(z)}{3} \quad (11) \\ & \frac{c^3(M, z)}{I_1(x_{min}, c(M, z))^2} I_2(x_{min}, c(M, z)). \end{aligned}$$

In the previous expression, the virial overdensity is [19]:

$$\Delta_{vir}(z) = \frac{18\pi^2 + 82(\Omega_m(z) - 1) - 39(\Omega_m(z) - 1)^2}{\Omega_m(z)}. \quad (12)$$

and the integrals  $I_1$  and  $I_2$  have an analytic expression:

$$I_n(x_{min}, x_{max}) = \int g^n x^2 dx, \quad (13)$$

where  $g(x) = x^{-1}(1+x)^{-2}$ .

In Eq. 11, the lower integration limit is set at the minimum radius within which the annihilation rate equals the dynamical time:  $x_{min} = 10^{-8} \text{kpc}/r_s$  ( $r_s$  is the scale radius in kpc). We have checked that the results are not sensitive to a different choice for  $x_{min}$ .

Putting Eqs. 11 and 10 together, we obtain the expression for the isotropic gamma-ray flux from extra-galactic DM halos:

$$\begin{aligned} & \left\langle \frac{d\Phi}{dE_0 d\Omega} \right\rangle (E_0) = \frac{\sigma v}{8\pi} \frac{c}{H_0} \frac{\rho_{cr}^2 \Omega_{0,m}^2}{m_\chi^2} \times \quad (14) \\ & \int dz (1+z)^3 \frac{\Delta^2(z)}{h(z)} \frac{dN_\gamma(E_0(1+z))}{dE} e^{-\tau(z, E_0)}, \end{aligned}$$

with

$$\Delta^2(z) = \int dM \frac{\nu(z, M) f(\nu(z, M))}{\sigma(M)} \left| \frac{d\sigma}{dM} \right| \Delta_M^2(z, M) \quad (15)$$

and

$$\Delta_M^2(z, M) = \int dc' P(c(M, z), c') \frac{\Delta_{vir}}{3} \frac{I_2(x_{min}, c')}{I_1^2(x_{min}, c')} (c')^3 dc'. \quad (16)$$

$\Delta_M^2(z, M)$  represents the enhancement in the gamma-ray flux due to the presence of a DM halo with a mass  $M$  at a redshift  $z$ . In  $\Delta^2(z)$  all these contributions are integrated over the halo mass function. Therefore  $\Delta^2(z)$  quantifies how much the annihilation signal is boosted up by the existence of virialized DM halos.

To account for the presence of substructures in extra-galactic halos, we assume that a given fraction of the halo mass is concentrated in substructures with the same properties as the galactic subhalos described in Section II. For consistency with the MW case, we require 10% of the parent halo mass  $M$  to be in subhalos in the mass range  $10^{-5}M - 10^{-2}M$ . Following this requirement the mass fraction  $f(M)$  in substructures within a host halo of mass  $M$  can be fitted as

$$f(M) \equiv \frac{M_s^{\text{tot}}}{M} = \frac{1}{6} + \frac{\log_{10}(M/M_\odot)}{30}. \quad (17)$$

With the above definition, the presence of substructures is taken into account replacing  $\Delta_M^2$  in Eq. 16 with the following expression:

$$\begin{aligned} \Delta_M^2(M) &\rightarrow (1 - f(M))^2 \Delta_M^2(M) + \quad (18) \\ & + \frac{1}{M} \int dM_s M_s \frac{dn}{dM_s}(M_s, z) \Delta_{M_s}^2(z, M_s). \end{aligned}$$

## IV. MAPPING THE GAMMA-RAY ANNIHILATION SIGNAL

### A. Galactic contributions

The gamma-ray flux from local substructures receives contributions from all the subhalos along the line of sight,

typically  $\sim 10^9$  subhalos when integrating over a solid angle  $\sim 10^{-5}$ sr. A brute-force integration with a Monte Carlo approach is therefore impossible even on high-speed computers. To circumvent this problem, Pieri et al. in Ref. [18] have proposed a hybrid approach that consists in splitting the integral into two different contributions. The first one, which we regard as due to unresolved subhalos, is the average contribution of a subhalo population distributed according to Eq. 5, which can be estimated analytically. The second one comes from the nearest subhalos, that one may hope to resolve as individual structures, and it is estimated by numerical integration of 10 independent Monte Carlo realizations. To determine the number of individual subhalos in each Monte Carlo realization we assume that their contribution to the gamma-ray flux represents a Poisson fluctuation to the mean gamma-ray annihilation signal. Following this criterion, we only consider, in each mass decade, subhalos with  $\Phi^{\text{cosmo}} > \langle \Phi_{B_{z_0,ref}}^{\text{cosmo}}(\psi = 180^\circ) \rangle \sim 10^{-5} \text{ GeV}^2 \text{ cm}^{-6} \text{ kpc sr}$ , where the brackets indicate the mean annihilation flux. For a given halo mass, this requirement corresponds to generate all subhalos within a maximum distance  $d_{max}(M)$ . More than 500 subhalos are found within  $d_{max}$  for each mass decade from  $10 M_\odot$  to  $10^7 M_\odot$  and their positions are simulated according to Eq. 5. For less massive subhalos, if less than 500 subhalos are found, we increase  $d_{max}$  to include all the nearest 500 subhalos in that mass range.

Pieri et al. in Ref. [18] have checked that the predicted gamma-ray flux does not depend on  $d_{max}$ . Here we need to perform a similar robustness test to check that the choice of  $d_{max}$  does not introduce spurious features in the angular power spectrum. For this purpose we have generated different Monte Carlo realizations simulating subhalos up to  $n \times d_{max}$  with  $n$  from 2 to 5. We have checked that convergence in the power spectra is obtained already for  $n = 2$ . Since the convergence depends weakly on the model concentration parameter adopted, in this paper we have adopted a more stringent criterion and set our maximum simulation distance at  $3 \times d_{max}(M)$  to guarantee that the convergence is reached in both subhalo models considered.

To summarize, in our model we consider three sources of gamma-ray annihilation within the MW: the smooth Galactic halo (which we will refer to as NFW), the unresolved subhalos (UNRES), and the resolved substructures (RES). Since the total annihilation depends on the square of the DM density, for the purpose of computing the angular correlation signal we also need to consider the double products NFW  $\times$  RES and NFW  $\times$  UNRES. We neglect RES  $\times$  UNRES since a resolved subhalo at a given location excludes the presence of unresolved substructures.

We point out that the subhalos labelled as "resolved" do not correspond to those substructures that will be detected by Fermi LAT. Instead they merely represent the nearest subhalos that we have generated to account for the discreteness of the subhalo spatial distribution.

Moreover, considering the population of RES subhalos also accounts for the pixel-to-pixel variation in the annihilation flux that would be neglected focusing only on the smooth UNRES signal.

The possibility of detecting galactic DM substructures is discussed in details in Ref. [18]. Since, in model  $B_{z_0,ref}$ , Fermi LAT is expected to detect only very few substructures, in this work all the simulated subhalos are included in the RES map. On the contrary, for model  $B_{z_f,ref}$ , Fermi LAT may resolved up to  $\sim 100$  point-like sources. Since we are interested in the correlation properties of the diffuse gamma-ray emission, these sources should be masked. However, we checked that the angular spectrum for the model  $B_{z_f,ref}$  does not significantly depend on the exclusion of these point-like sources.

In Figures 1 and 2 we show the different contributions to the differential flux at 10 GeV as a function of the angle  $\Psi$  from the GC in model  $B_{z_0,ref}$  and  $B_{z_f,ref}$ , respectively.

For  $B_{z_0,ref}$  (Fig. 1) the flux from galactic substructures (red curve) dominates over the smooth NFW profile (black curve) at angular distances from the GC larger than about  $3^\circ$  and it remains the dominant contribution at larger angles. The blue line labeled 'EGRET' represents the EGB inferred from EGRET measurements, equal to  $1.10 \times 10^{-8} \text{ cm}^{-2} \text{ s}^{-1} \text{ GeV}^{-1} \text{ sr}^{-1}$  at 10 GeV, that can be used as a generous upper bound (the Fermi LAT satellite will impose more stringent constraints, see next section).

Note that the NFW curve in Fig. 1 exceeds the EGRET EGB in the central degree, but not the flux of the bright gamma-ray source (J1746-2851) that has been identified by EGRET to be near - possibly coincident with - the GC, and it is thus consistent with observations.

For  $B_{z_f,ref}$ , galactic substructures dominate the NFW signal at even smaller angular separations from the GC. In this case, the average flux for galactic substructures is larger than in the  $B_{z_0,ref}$  case and almost matches the EGRET background.

## B. Extra-galactic contribution

The green line in Figures 1 and 2 represents the average extra-galactic flux contributed by DM annihilation in extra-galactic halos, and their substructures, calculated with Eq. 14. In model  $B_{z_0,ref}$  this flux turns out to be  $2.20 \times 10^{-11} \text{ cm}^{-2} \text{ s}^{-1} \text{ GeV}^{-1} \text{ sr}^{-1}$ , significantly smaller than in model  $B_{z_f,ref}$  (for which it is  $1.45 \times 10^{-10} \text{ cm}^{-2} \text{ s}^{-1} \text{ GeV}^{-1} \text{ sr}^{-1}$ ) but still well below the galactic contribution and the EGRET constraint.

We stress the fact that in this work we have considered the EGRET background since it constitutes the best observational constraint available to date. This background is likely to be dominated by unresolved extra-galactic sources like blazars. Using the blazars Gamma-ray Luminosity Function derived from the blazars detected by EGRET, Ando et al. have shown that these sources should contribute only to 25-50% of the total EGB [13].

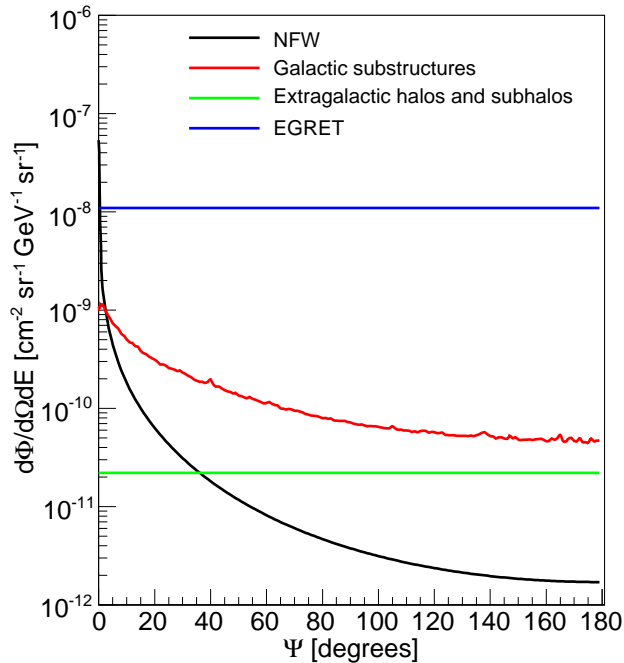


FIG. 1: Different contributions to the differential flux  $d\Phi/dEd\Omega$  [ $\text{cm}^{-2}\text{s}^{-1}\text{GeV}^{-1}\text{sr}^{-1}$ ] at 10 GeV as a function of the angle  $\Psi$  from the GC, in model  $B_{z_0,ref}$ . The blue line corresponds to the EGRET estimate of the EGB as parametrized in Ref. [15]. The contribution from DM annihilation in the smooth host halo and its substructures are represented by the black and red curves, respectively. The latter is obtained by averaging over 10 different Monte Carlo realizations of the subhalos population. Bumps and wiggles are due to the contribution of the individual subhalos of the RES population. The green line represents the extra-galactic flux contributed by DM annihilation within extra-galactic halos and their substructures. We have assumed  $m_\chi = 40$  GeV,  $\sigma v = 3 \times 10^{-26} \text{cm}^3 \text{s}^{-1}$  and annihilations to  $b\bar{b}$ .

One therefore expects that, thanks to its superior sensitivity, Fermi LAT will be able to resolve a significant fraction of these sources [39]. As a result, the amplitude of the unresolved gamma-ray background will decrease, effectively lowering the blue line in Figs. 1 and 2 in the case of Fermi LAT. This will have three advantages. First of all, a fainter gamma-ray background will increase the probability of detecting the gamma-ray annihilation signal produced by individual structures. Second, the background from Fermi LAT will provide tighter constraints to our model for the DM annihilation, telling us if our description is too optimistic. Finally, with a larger number of resolved astrophysical sources, Fermi LAT will provide a better estimate of the blazar luminosity function.

The fact that the extra-galactic flux is contributed by both DM annihilation and blazars and because of the uncertainty on the latter contribution, one has the freedom of modifying the relative importance of blazars emission to the total EGB, keeping a good agreement with the data. Different choices for these relative contributions

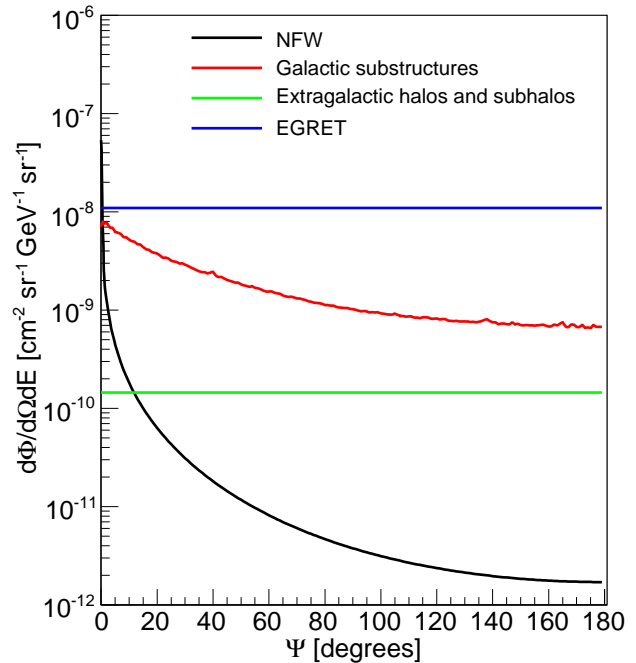


FIG. 2: Different contributions to the differential flux  $d\Phi/dEd\Omega$  at 10 GeV as a function of the angle  $\Psi$  from the GC in model  $B_{z_f,ref}$ . The curves represents the same quantities shown in Fig. 1 but for  $B_{z_f,ref}$ .

have been proposed in Ref. [13]. They are listed in the first two columns of Tab. II. The same DM annihilation flux leads to a different value of  $f_{\text{DM}}^{\text{EGRET}}$  for EGRET and Fermi LAT, due to the lower Fermi LAT EGB.

It is particularly important to note that not all of the scenarios in Tab. II are physically plausible when implemented in our model. For example, boosting the average galactic and extra-galactic DM annihilation flux so that it will account for more than 61% of the Fermi LAT EGB, leads to a flux that exceeds the EGRET constraint towards the GC (even excluding the central degree). Thus, for  $B_{z_0,ref}$  we will only consider  $f_{\text{DM}}^{\text{Fermi}}$  as large as 0.61, restricting to the last two rows in Tab. II. For the model  $B_{z_f,ref}$ , a similar argument rules out cases with  $f_{\text{DM}}^{\text{Fermi}} > 0.80$ .

## V. ANGULAR POWER SPECTRUM OF THE GAMMA-RAY UNRESOLVED SIGNAL

### A. Galactic contribution

To compute the galactic gamma-ray angular power spectrum and investigate the relative importance of the different contributions, we separately analyze the five maps of  $\Phi^{\text{cosmo}}$  corresponding to the NFW, RES, UNRES, NFW×RES and NFW×UNRES contributions. In the maps, the value of  $\Phi^{\text{cosmo}}$  is specified within angular

| $f_{\text{blazars}}^{\text{EGRET}}$ | $f_{\text{DM}}^{\text{EGRET}}$ | $f_{\text{blazars}}^{\text{Fermi}}$ | $f_{\text{DM}}^{\text{Fermi}}$ | b.f. $B_{z_0,ref}$ | b.f. $B_{z_f,ref}$ |
|-------------------------------------|--------------------------------|-------------------------------------|--------------------------------|--------------------|--------------------|
| 0.1                                 | 0.9                            | 0.03                                | 0.97                           | ruled out          | ruled out          |
| 0.3                                 | 0.7                            | 0.20                                | 0.80                           | ruled out          | 5.9                |
| 0.5                                 | 0.5                            | 0.39                                | 0.61                           | 49.8               | 4.2                |
| 0.7                                 | 0.3                            | 0.61                                | 0.39                           | 29.9               | 2.6                |

TABLE II:  $f_{\text{blazars}}^{\text{EGRET}}$  and  $f_{\text{DM}}^{\text{EGRET}}$  indicate the contribution of gamma-ray from blazars and from DM annihilation respectively, to the EGB as measured by EGRET.  $f_{\text{blazars}}^{\text{Fermi}}$  and  $f_{\text{DM}}^{\text{Fermi}}$  represent the same quantities estimated for the Fermi LAT satellite in Ref. [13] using the blazar luminosity function derived from EGRET data. The last two rows indicates the corresponding boost factors needed to bring the average annihilation flux (galactic plus extra-galactic) to the relative percentage of the EGB value.

bins of  $\Delta\Omega = 9.57 \times 10^{-6} \text{sr}$ .

Since we are interested in the contributions of DM halos and subhalos, we mask out the region close to the GC and the Galactic plane in which the signal is dominated by gamma-rays produced by cosmic rays interacting with the interstellar galactic medium [14]. This background rapidly decreases with galactic latitude. For this reason we have used a composite mask consisting in a strip of  $10^\circ$  above and below the Galactic plane and the squared area around the GC with coordinates  $|b| \leq 30^\circ$  and  $|l| \leq 30^\circ$ . Outside the mask, the average galactic annihilation flux turns out to be  $\langle d\Phi/dEd\Omega \rangle = 8.79 \times 10^{-11} \text{cm}^{-2} \text{s}^{-1} \text{GeV}^{-1} \text{sr}^{-1}$  in the case of  $B_{z_0,ref}$  and  $\langle d\Phi/dEd\Omega \rangle = 1.16 \times 10^{-9} \text{cm}^{-2} \text{s}^{-1} \text{GeV}^{-1} \text{sr}^{-1}$  for  $B_{z_f,ref}$ , and it is dominated by the UNRES term.

To characterize the angular correlation signatures of the various contributions we compute the angular power spectrum of the different maps with the **HEALPix** 2.01 package [40, 41]. Five **Healpix\_Map** objects are created covering the whole sky with 786432 pixels of constant area (corresponding to `N_side` = 2<sup>8</sup>). Each pixel of the **Healpix\_Map** is filled with the corresponding flux  $d\Phi/dEd\Omega$  from the simulated maps. The number of pixels is determined from the requirement that the area of the single bin is smaller than  $\Delta\Omega$ .

The angular power spectrum,  $C_\ell$ , is computed from the spherical harmonic coefficients  $a_{\ell,m}$  of the gamma-ray flux angular fluctuation map as follows:

$$\left\langle \frac{d\Phi}{dEd\Omega} \right\rangle a_{\ell,m} = \int d\Omega \left( \frac{d\Phi(\theta, \phi)}{dEd\Omega} - \left\langle \frac{d\Phi}{dEd\Omega} \right\rangle \right) Y_{\ell,m}(\theta, \phi)^*, \quad (19)$$

$$C_\ell = \frac{\sum_{m=0}^{\ell} |a_{\ell,m}|^2}{2\ell + 1}, \quad (20)$$

where  $Y_{\ell,m}(\theta, \phi)$  are the spherical harmonics and the integration in Eq. 19 extends to the unmasked area. The angular spectra of the RES and NFW×RES maps have been obtained by averaging the spectra of the 10 independent maps corresponding to the different Monte Carlo realizations of resolved subhalos.

We note in passing that the angular correlation signal does not depend on the particle physics scenario since it is evaluated with respect to the average flux (aside from a weak dependence on the minimum subhalo mass, which in turn depends on the properties of the DM particle). However, for the purpose of comparing the gamma-ray angular spectrum due to DM annihilation to that of extra-galactic astrophysical sources, a particular particle physics scenario has to be specified. In this case we refer to the reference values presented in Section III A.

Our masking procedure induces spurious features in the NFW, UNRES and NFW×UNRES spectra that we smoothed out by averaging over 18 multipoles.

The total angular spectrum is obtained by performing a sum of the aforementioned contributions and the cross-correlation terms:

$$\left\langle \frac{d\Phi^{\text{tot}}}{dEd\Omega} \right\rangle^2 C_\ell^{\text{tot}} = \sum_i \left\langle \frac{d\Phi^i}{dEd\Omega} \right\rangle^2 C_\ell^i + \sum_{i,j} \left\langle \frac{d\Phi^i}{dEd\Omega} \right\rangle \left\langle \frac{d\Phi^j}{dEd\Omega} \right\rangle \sum_m a_{\ell,m}^i a_{\ell,m}^{*j}, \quad (21)$$

with  $i, j \in [\text{NFW}, \text{RES}, \text{UNRES}, \text{NFW} \times \text{RES}, \text{NFW} \times \text{UNRES}]$ .

The results for model  $B_{z_0,ref}$  are plotted in Fig. 3, for which we also have taken into account the pixel window function for the corresponding resolution of our maps [41]. The different curves in the plot represent the angular spectrum of each component weighted by the square of its relative contribution to the total annihilation flux  $\langle d\Phi^i/dEd\Omega \rangle^2 / \langle d\Phi^{\text{tot}}/dEd\Omega \rangle^2$ . Cross-correlations are taken into account in the computation of the total spectrum but are not shown in Figs. 3 and 4. Black crosses represent the spectrum of the total flux and the shaded areas show the  $1\sigma$  error boxes. These are obtained by summing in quadrature the uncertainties related to the finite bin size and, if applicable, the scatter among the different Monte Carlo realizations of resolved subhalos. The first contribution dominates at lower multipoles  $\ell$  while the second becomes the main source of error at larger multipoles where the power spectrum is mainly due to the RES contribution. Poisson errors are not accounted for since they depend on the observational setup and they will be discussed in the next Section for the case of the Fermi LAT satellite.

The main contribution to the total flux is provided by the autocorrelation of the resolved (red curve) and unresolved (blue curve) subhalos. The former dominates at large multipoles while the latter dominates at  $\ell < 30$ . The interplay between these two components is responsible for the minimum at  $\ell \sim 30$  in the total spectrum. All components involving the smooth DM distribution provide a negligible contribution to the total spectrum.

Fig. 4 shows the angular spectrum of model  $B_{z_f,ref}$ . The total spectrum and the different contributions are very similar to model  $B_{z_0,ref}$ . The only difference is represented by the position of the minimum which is now around  $\ell \sim 50$ . This is due to the contribution of the



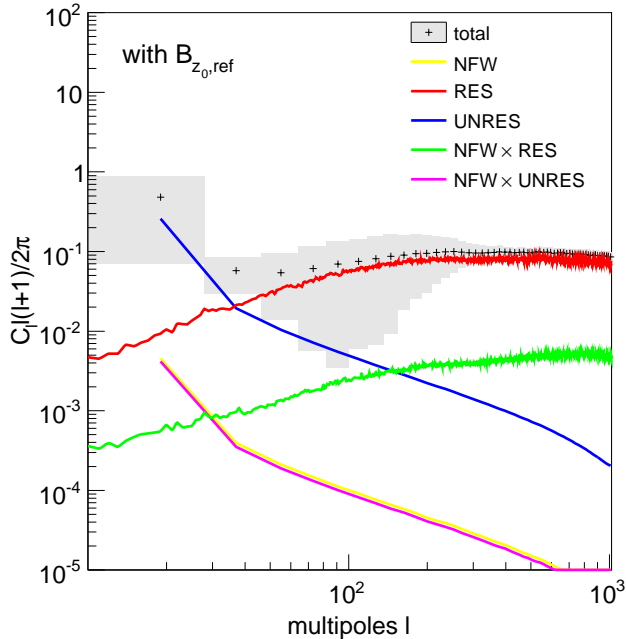


FIG. 3: The curves represent the angular power spectrum  $C_\ell \ell(\ell+1)/2\pi$  of the different contributions to the galactic annihilation flux in the framework of model  $B_{z_0,ref}$ . The labels identify the different contributions. Black crosses represent the angular spectrum of the total annihilation signal together with its  $1\sigma$  error (shaded areas).

resolved subhalos (red curve) which is smaller than in the previous case: subhalos in the  $B_{z_f,ref}$  model are less concentrated than in  $B_{z_0,ref}$  and consequently they contribute less to the spectrum at small angular scales. We conclude that changing the concentration parameter significantly affects the mean annihilation flux but not the angular power spectrum of the signal.

Our model predictions depend on the assumption about the minimum subhalo mass, for which the theory does not provide very strong constraints. In order to check the dependence of our results on the minimum subhalo mass, we have re-simulated the resolved subhalos excluding all structures below a given mass threshold. The spectrum does not change when excluding subhalos with a mass below  $10^4 M_\odot$ , showing that the angular correlation is mainly contributed by massive subhalos.

To check the reliability of our hybrid model, we have compared our results with those of a similar study recently carried out by Siegal-Gaskins [21] who used a pure Monte Carlo approach to compute the power spectrum of the annihilation signal produced by a population of subhalos in the MW above  $10 M_\odot$  and  $10^7 M_\odot$ , hence neglecting the contribution of smaller subhalos. To compare our simulation approach to hers, we have modified our subhalo model to match that of Ref. [21]. In particular we have re-simulated our galactic subhalo using a shallower mass function  $dn/dM \propto M^{-1.9}$ , assuming an Einasto density profile  $\rho_{halos}$  for subhalos, adopted a

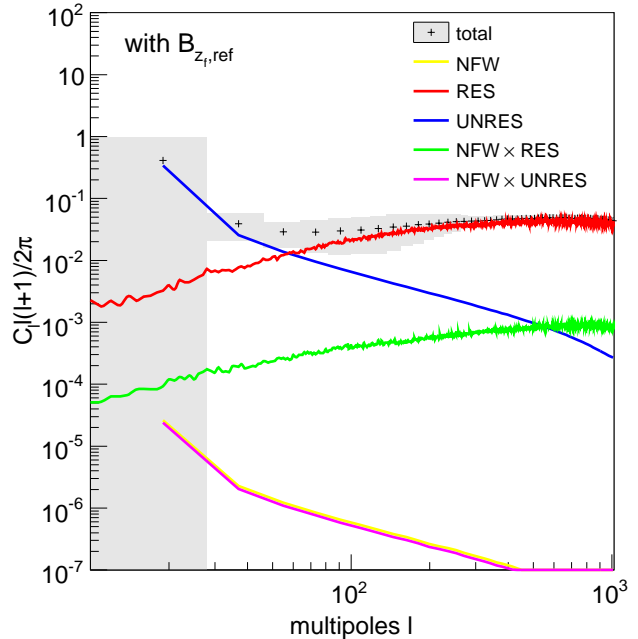


FIG. 4: The curves represent the angular power spectrum  $C_\ell \ell(\ell+1)/2\pi$  of the different contributions to the galactic annihilation flux in the framework of model  $B_{z_f,ref}$ .

simplified power-law model for the concentration parameter with  $c(M) \propto M^{-0.138}$  and normalized the number of subhalos in the MW with a mass larger than  $10^8 M_\odot$  to be  $N(M > 10^8 M_\odot) = 0.0064(10^8 M_\odot/M_{MW})^{-0.9}$  (this normalization forces the number of MW subhalos to be five times smaller than with the normalization assumed in Sec. II for the  $B_{z_0,ref}$  and  $B_{z_f,ref}$  cases).

The only residual difference between our model and that of Fig. 5 and 6 of Ref. [21] is the spatial subhalo distribution in the MW which is more similar to the anti-biased model of Ref. [21].

The result of this exercise is shown in Fig. 5. The curves shows the spectra normalized at  $C_\ell = 150$  for the various cases explored. The spectra of the subhalos *a la* Siegal-Gaskins are consistent with Fig. 5 and 6 of Ref. [21] for both the two mass thresholds considered ( $10 M_\odot$  (black curve) and  $10^7 M_\odot$  (red curve)). The agreement is valid at the same time for the shape and the amplitude of the signals.

The comparison with the spectrum of our subhalos in the case of  $B_{z_0,ref}$ , shows that, for the same mass cut, our spectrum is steeper than in Ref. [21]. This can be explained by noticing that small mass halos are more concentrated in Ref. [21] than in our case, resulting in a larger power at small scales (i.e. at large multipoles).

Also the amplitude of the angular spectra predicted in models  $B_{z_0,ref}$  and  $B_{z_f,ref}$  results to be different than the same quantity in Fig. 5 of Ref. [21], even when the different subhalo spatial distribution is considered: our spectra are characterized by a lower amplitude, the

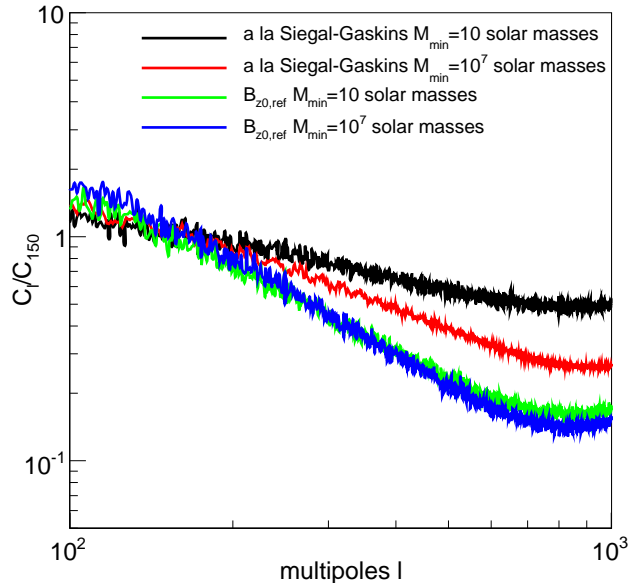


FIG. 5: Angular power spectrum  $C_\ell$ , normalized to  $C_{150}$  for the resolved subhalos modeled as in Ref. [21]. The black (red) curve shows the case of a  $10M_\odot$  ( $10^7M_\odot$ ) mass cutoff. The green (blue) curve indicates the spectrum for the resolved subhalos in model  $B_{z_0,ref}$  for a mass cutoff of  $10M_\odot$  ( $10^7M_\odot$ ).

result of having considered subhalos with masses lower than  $10M_\odot$ . They contribute to the total annihilation flux but their distribution is almost homogeneous around the observer, hence decreasing the spectral amplitude.

Finally, as we have already pointed out, the results presented here are robust to the choice of the maximal simulation distance. We have checked that resolving halos at distances larger than  $3 \times d_{max}(M)$  has very little impact on the angular power spectrum.

### B. Extra-galactic contribution

Our analysis for the angular spectrum of the extra-galactic annihilation flux is similar to the one originally developed by Ando et al. in Ref. [12] and extended in [13] to account for substructures. Like in our model, these authors assume that DM halos and subhalos have NFW density profiles and that subhalos trace the smooth underlying mass distribution of the host halo. Moreover they assume that the mean number of subhalos within a host halo of mass  $M$ ,  $\langle N|M \rangle$ , scales as  $\propto M^\alpha$  and they consider two extreme cases,  $\alpha = 1$  and  $\alpha = 0.7$  [13]. In this work we only consider the first case to match the subhalo mass function of our model.

We notice that Ando et al. [13] do not account for the contribution of subhalos by integrating over their mass function, as in the second term of Eq. 18. Instead, they consider a gamma-ray subhalo spectrum averaged over

its mass function and multiplied by the mean comoving density of subhalos. These model details hardly affect the angular power spectrum since one considers fluctuations about the mean flux. While we will quantify the differences between the two approaches in a future work in which the angular power spectrum and the mean flux will be computed self-consistently, here, for the purpose of discussing the angular power spectrum, we adopt the same approach as in Ref. [13] and we will use their very same angular power spectra shown in Fig. 5 of their paper for both the DM annihilation and the blazars contribution to the extra-galactic flux.

We do not plot the contribution of the DM and blazars to the angular spectrum of the extra-galactic gamma-ray background in Figs. 3 and 4 to avoid confusion. Instead, in the next Section we show how well these spectra will be measured by Fermi LAT and compare them to the galactic contributions.

## VI. FERMI LAT GAMMA-RAY ANGULAR SPECTRA

In this section we apply our model to predict the angular power spectrum that Fermi LAT is expected to observe and discuss the possibility of indirect DM detection through characteristic signatures in the spectrum.

The contribution of the different components to the total angular spectrum of the gamma-ray flux is shown in Fig. 6 for the  $B_{z_0,ref}$  case. The red histogram indicates the angular spectrum of anisotropies in the blazar emissivity (see Fig. 5 of Ref. [13]). Black crosses represents the contribution of galactic substructures that, as we have shown, dominate over the smooth NFW signal. Open diamonds indicate the contribution of extra-galactic halos and their substructures. All the different contributions are normalized to the square of the ratio between the average flux of that particular contribution to the average total flux  $\langle d\Phi^i/dEd\Omega \rangle^2 / \langle d\Phi^{tot}/dEd\Omega \rangle^2$ .

Poissonian errors in each bin of the sky maps are due to the small statistics, i.e. the limited number of gamma-ray photons from annihilation collected during observations. The  $1\sigma$  error is computed, following Ref. [13], as follows:

$$\delta C_l = \sqrt{\frac{2}{(2l+1)\Delta l f_{t.o.v.}}} \left( C_l + C_l^b + \frac{C_N}{W_l^2} \right), \quad (22)$$

where  $\Delta l = 18$  and  $4\pi f_{t.o.v.} = 9.706$  sr is the area outside the mask.  $C_N$  is the power spectrum of the photon noise  $C_N = 4\pi f_{t.o.v.}/N_{EGB}$  that depends on the instrument characteristics and integration time ( $N_{EGB}$  is the number of photons of the EGB) and is independent from  $\ell$ . We have assumed an effective area constant with energy of  $10^4 \text{cm}^2$  and an exposure time of 1 year.  $W_\ell$  is the window function of a Gaussian point spread function  $W_\ell = \exp(-\ell^2 \sigma_b^2/2)$  that we compute for the Fermi LAT angular resolution  $\sigma_b = 0.115^\circ$ . The angular spectrum of the background  $C_\ell^b$  is not uniquely defined but depends

on the signal one wants to detect: for the extra-galactic DM component, the background is represented by blazars and by the galactic annihilations. While, viceversa, for the galactic DM component, blazars and extra-galactic annihilations play the role of background.

The total signal (shown as crosses in Fig. 6 and Fig. 7) is obtained by adding all components weighted by their relative contribution to the total gamma-ray flux  $\langle d\Phi^i/dEd\Omega \rangle^2 / \langle d\Phi^{\text{tot}}/dEd\Omega \rangle^2$  including the cross-correlation term involving extra-galactic halos and blazars. We have ignored the cross-correlation between the galactic subhalos and the blazars since they have independent spatial distributions. The total errors (blue boxes) account for the Poisson noise of both the galactic and extra-galactic DM component, to which we summed the binsize and scatter among Monte Carlo realizations. The Poissonian noise becomes the main source of errors only at large multipoles. Finally, we have assumed that the angular power spectrum of blazars is known without errors.

In the particle physics scenario considered in this paper and for the  $B_{z_0,ref}$  model, the average flux  $\langle d\Phi/dEd\Omega \rangle$  produced by DM annihilations within and outside our galaxy is less than 1% of the EGB estimated for Fermi LAT. We can therefore boost up this contribution by increasing the cross section of the DM candidate. This has the effect of changing the values of  $f_{\text{blazars}}^{\text{Fermi}}$  and  $f_{\text{DM}}^{\text{Fermi}}$ , i.e. the relative contribution of blazars and DM to the total EGB. The two panels in Figure 6 refer to  $f_{\text{DM}}^{\text{Fermi}} = 0.61$  (left) and  $f_{\text{DM}}^{\text{Fermi}} = 0.39$  (right). The corresponding boosting factors are shown in the plots. Larger boosting factors (corresponding to larger  $f_{\text{DM}}^{\text{Fermi}}$ ) are excluded since they would correspond to models already excluded by the current EGRET constraint.

In both plots the contribution of the galactic signal to the angular power spectrum largely dominates the extra-galactic component at all multipoles. As a consequence, the two main contributions to the angular spectrum are provided by the blazars and the galactic annihilation signal. The former dominates at large multipoles whereas the latter dominates at low  $\ell$ . The position of the crossover depends on the boosting factor, but even in the less favorable case of  $f_{\text{DM}}^{\text{Fermi}} = 0.39$  the DM annihilation signature can be clearly seen as a turnover in the power spectrum at  $\ell < 30$ .

These considerations remain valid for the  $B_{z_f,ref}$  model whose angular power spectrum is shown in Fig. 7. In this case, however, the crossover is found at smaller multipoles, making more difficult to detect the contribution for DM annihilation when  $f_{\text{DM}}^{\text{Fermi}} = 0.39$  because of the large errorbars. On the other hand, with the  $B_{z_f,ref}$  model one can increase the boost factor up to  $f_{\text{DM}}^{\text{Fermi}} = 0.80$  without ending up with an unphysical scenario already excluded by EGRET.

## VII. DISCUSSION AND CONCLUSIONS

In this paper we have modeled for the first time the angular power spectrum of the diffuse gamma-ray signal at high galactic latitude taking into account both the DM annihilation in substructures within our Galaxy and annihilation within extra-galactic halos and their subhalos, also including the contribution from extra-galactic objects like blazars. The purpose is to understand whether the gamma-ray satellite Fermi LAT will be able to unambiguously detect the signature of DM annihilation that, in the  $\Lambda$ CDM scenario, preferentially takes place in the central regions of DM halos and in their hierarchically-nested substructures.

For this purpose we have developed an hybrid approach in which the annihilation signal is computed using two different techniques. First, we perform a numerical integration to compute the contributions to the gamma-ray flux from the smooth galactic halo, from the unresolved galactic substructures and, finally, from extra-galactic DM halos and their substructures. Second, we use Monte Carlo techniques to account for the nearest galactic subhalos, that show up in the mock gamma-ray maps as individual gamma-ray sources.

We have explored two different subhalo models corresponding to different prescriptions for the mass concentration within the halo,  $B_{z_0,ref}$  and  $B_{z_f,ref}$ .

The EGB is computed by adding the annihilation signal from extra-galactic halos and that from high energy astrophysical sources like blazars. The relative contributions of the two signals is treated as a free parameter. The only constraint is that the total gamma-ray signal, galactic annihilation foreground and EGB, does not exceed the current limit of EGRET.

Our main conclusions are:

- The annihilation of the smooth galactic halo dominates over that of galactic substructures only within a few degrees from the GC. The exact value depends on the subhalos concentration and ranges from  $< 1^\circ$  in model  $B_{z_f,ref}$ , to  $\sim 3^\circ$  in model  $B_{z_0,ref}$ . Moreover, the gamma-ray flux from extra-galactic halos is fainter than the galactic signal at all angles. This is true both for  $B_{z_0,ref}$  and  $B_{z_f,ref}$ .
- To predict the annihilation flux we have assumed a favourable particle physics setup, with a mass of 40 GeV, a cross section  $\sigma v = 3 \times 10^{-26} \text{ cm}^{-3} \text{ s}^{-1}$ , and annihilations to  $b\bar{b}$ . With this choice, model  $B_{z_0,ref}$  accounts for only 0.8% of the total unresolved EGB that will be measured by Fermi LAT. Larger fluxes are possible for smaller masses and larger cross sections, provided that the total flux does not exceed the current measurement of the EGB by EGRET and still allowing blazars to contribute to a significant fraction of the flux. Similar considerations also apply to model  $B_{z_f,ref}$ . The largest boost factor compatible with the data is of order 100, and it

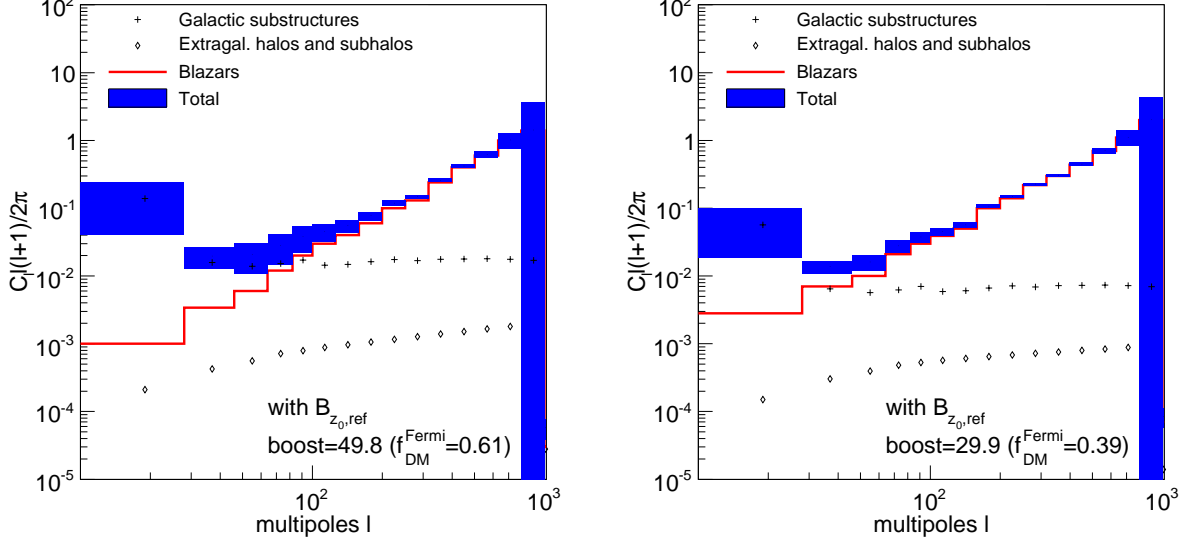


FIG. 6: Angular power spectrum of gamma-ray anisotropies in the case that DM annihilations contribute to 61% (left) and 39% (right) of the total average flux of the EGB as estimated for the Fermi LAT satellite. The plus signs + indicate the galactic component following the  $B_{z_0,ref}$  model (see Fig. 3). The diamonds  $\diamond$  refer to DM annihilating in extra-galactic, unresolved DM halos and subhalos and the spectrum is taken from Ref. [13]. The red line represents the angular spectrum of blazars as described in Ref. [13]. All these three components are normalized to their average contribution to the total flux  $\langle d\Phi^i/dE d\Omega \rangle^2 / \langle d\Phi^{tot}/dE d\Omega \rangle^2$ . The  $1\sigma$  error of the total spectrum is indicated by the blue boxes and it is obtained propagating the errors from the galactic and the extragalactic DM components, assuming no errors for the blazars.

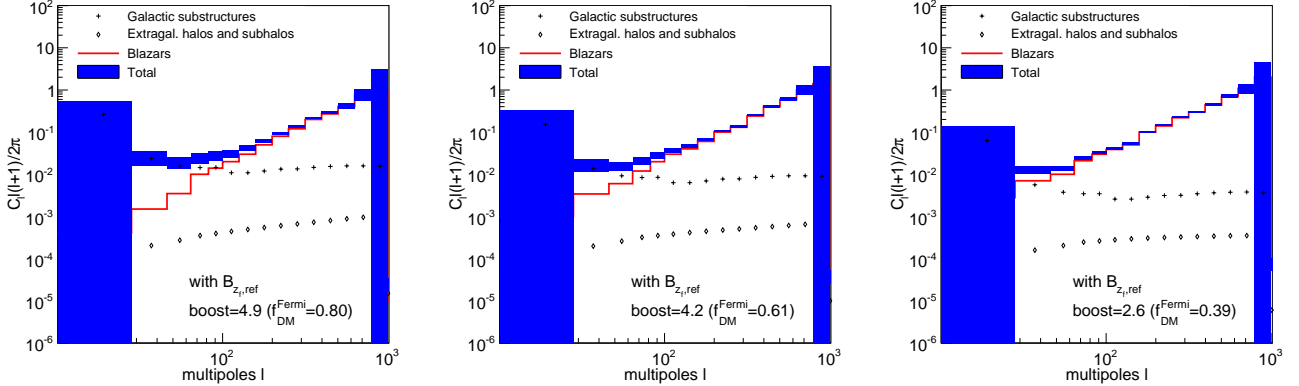


FIG. 7: Angular power spectrum of gamma-ray anisotropies in the case that DM annihilations contribute to 80% (left), 61% (center) and 39% (right) of the total average flux of the EGB as estimated for the Fermi LAT satellite. The curves and the error boxes have the same meaning of Fig. 6 but refer here to the  $B_{z_f,ref}$  case.

could be achieved e.g. through the so-called Sommerfeld enhancement or in some rather fine-tuned supersymmetric scenarios [42, 43].

- The angular power spectrum predicted by our model is reliable and robust. To test its reliability we compared our results with those recently published in Ref. [21], who performed a similar analysis considering, however, only galactic substructures and using a full Monte Carlo approach. When the

same halo model is considered, we find fair agreement with Ref. [21]. To test the robustness of our method we have verified that our results do not change significantly when we increase the volume within which we simulate the distribution of galactic subhalos beyond a well defined reference value.

- The angular power spectrum of the galactic gamma-ray photons produced by DM annihilation is dominated by subhalos. Contributions involv-

ing the DM particles in the smooth galactic halo are negligible at all multipoles. At low multipoles (large angles) the spectrum is dominated by unresolved halos whose annihilation flux appear in the gamma-ray sky map as a smooth foreground (see e.g. Figs. 6 and 7 of Ref. [18]). On the other hand, nearby resolved clumps dominate the power at small angular separations (large multipoles). These results are robust in the sense that they do not change appreciably when adopting different prescriptions for the concentration parameters. This is not surprising since the power spectrum, which refers to fluctuations about the mean flux, should not depend appreciably on the subhalo structure.

- Subhalos of masses below  $10^4 M_\odot$  give a small contribution to the angular spectrum of the galactic annihilation flux.
- The signature of DM annihilations in the angular power spectrum can be found only for an optimistic particle physics setup. In fact, for our benchmark particle physics scenario (without any boost factor) the power spectrum of the unresolved gamma-ray background would be completely dominated by blazars. However, boosting up the particle physics factor without exceeding the background that EGRET has estimated, we find that the power spectrum is dominated by the DM component at low multipoles while blazars determine the spectrum at small angular scales. The turn-over depends on the prescription for the concentration of subhalos, occurring at smaller scales in the case of  $B_{z_0,ref}$ .
- The angular power spectrum of DM annihilations is largely dominated, at all scales, by the galactic signal. It depends mostly on the relative importance of the average galactic flux compared to the extra-galactic DM signal which, in our models, favours the first term, both for  $B_{z_0,ref}$  and  $B_{z_f,ref}$ .
- We find that a 1-year all-sky survey with Fermi LAT, now operational, may be able to spot the annihilation signature of DM in the angular power spectrum of the unresolved gamma-ray flux. This signature is provided by the up-turn in the power spectrum which, at low multipoles, is dominated by the DM annihilation signal. Our results partially contradict those of Ref. [13] who did not account for the galactic contribution to the angular power spectrum which, instead, completely obliterate the one provided by annihilations in extra-galactic halos.
- Our results seem to confirm those of Ref. [21] since the angular spectrum measured by Fermi LAT should indeed provide an indirect detection from DM annihilation within our Galaxy, although it

is doubtful that such measurement will be able to constrain the properties of the subhalo population. However, we should point out that the subhalo description adopted in Ref. [21] would boost up the extra-galactic DM annihilation flux to a value of  $3.60 \times 10^{-10} \text{cm}^{-2} \text{s}^{-1} \text{GeV}^{-1}$  comparable to, if not larger than, the galactic annihilation flux. On one side this fact increases the possibility of detecting the DM contribution to the angular spectrum. On the other hand it will be hard to disentangle galactic and extra-galactic contributions.

As a remark we stress that the results of the recent *Via Lactea II* [30] and the *Aquarius* [31, 32] numerical experiments, both with improved resolution, have now updated our knowledge on the subhalo distribution function and concentration parameters. The differences in the subhalos extracted from these simulations, whose main characteristics are listed in Table I, may change the angular spectrum of the DM annihilation flux although we have shown that changing subhalo model significantly affects the gamma-ray flux but has less impact on the spectral analysis. We will investigate this issue thoroughly in a forthcoming paper. Here we just report the result of a preliminary analysis in which we have computed the angular power spectrum of the galactic annihilation signal obtained when subhalos are modeled according to *Via Lactea II* and *Aquarius*. In both cases we find that the angular spectrum is flatter, especially at small  $\ell$ . This is not surprising since, in both experiments, the mass distribution is less clumpy and the subhalo radial distribution is flatter than in the model adopted in the present paper. A flatter spectrum, combined with a fainter annihilation flux due to the reduced number of substructures, would reduce the up-turn in the angular spectrum, making it more challenging to detect the DM annihilation feature. The significance of this effect depends on the boosting factors that, because of the dimmer flux, could be further increased without exceeding the measured gamma-ray background.

Finally, being tuned to the results of N-body simulations, our description of the galactic and extra-galactic subhalo population does not account for the effect of baryons in the evolution of DM structures. As a consequence our computation of the angular spectrum does not account for the effect, e.g., of Intermediate Mass Black Holes, which may be present in our Galaxy and which correlation properties have been recently studied in Ref. [44].

## Acknowledgments

We would like to thank S. Ando, M. Gustafsson, E. Komatsu and J. Siegal-Gaskins for very useful comments on the manuscript. We would also like to thank M. Taoso for useful discussions and S. Ricciardi and E. Hivon for the help with the **HEALPix** package. LP would like to

thank the European Network of Theoretical Astroparticle Physics ENTApP ILIAS/N6 under contract number RII3-CT-2004-506222 for financial support. EB thanks

the Institut d'Astrophysique de Paris for the kind hospitality and acknowledge financial contribution from contracts ASI-INAF/TH-014 and ASI-INAF/TH-027.

- 
- [1] G. Bertone, D. Hooper and J. Silk, Phys. Rept. **405** (2005) 279 [arXiv:hep-ph/0404175].
- [2] L. Bergstrom, Rept. Prog. Phys. **63**, 793 (2000) [arXiv:hep-ph/0002126].
- [3] H. A. Mayer-Hasselwander *et al.*, Astron. Astrophys. **335** (1998) 161.
- [4] A. Cesarini, F. Fucito, A. Lionetto, A. Morselli and P. Ullio, Astropart. Phys. **21**, 267 (2004) [astro-ph/0305075].
- [5] D. Hooper and B. L. Dingus, Phys. Rev. D **70** (2004) 113007 [astro-ph/0210617].
- [6] F. Aharonian *et al.* [H.E.S.S. Collaboration], Phys. Rev. Lett. **97** (2006) 221102 [Erratum-ibid. **97** (2006) 249901] [arXiv:astro-ph/0610509].
- [7] G. Bertone and D. Merritt, Phys. Rev. D **72** (2005) 103502 [astro-ph/0501555].
- [8] P. Gondolo and J. Silk, Phys. Rev. Lett. **83**, 1719 (1999) [arXiv:astro-ph/9906391].
- [9] L. Bergstrom, P. Ullio and J. H. Buckley, Astropart. Phys. **9** (1998) 137 [arXiv:astro-ph/9712318].
- [10] L. Bergstrom, T. Bringmann, M. Eriksson and M. Gustafsson, JCAP **0504** (2005) 004 [arXiv:hep-ph/0412001].
- [11] T. Bringmann, L. Bergstrom and J. Edsjo, JHEP **0801** (2008) 049 [arXiv:0710.3169 [hep-ph]].
- [12] S. Ando and E. Komatsu, Phys. Rev. D **73** (2006) 023521 [arXiv:astro-ph/0512217].
- [13] S. Ando, E. Komatsu, T. Narumoto and T. Totani, Phys. Rev. D **75** (2007) 063519 [arXiv:astro-ph/0612467].
- [14] A. W. Strong, I. V. Moskalenko and O. Reimer, Astrophys. J. **537** (2000) 763 [Erratum-ibid. **541** (2000) 1109] [arXiv:astro-ph/9811296].
- [15] P. Sreekumar *et al.* [EGRET Collaboration], Astrophys. J. **494** (1998) 523 [arXiv:astro-ph/9709257].
- [16] A. W. Strong, I. V. Moskalenko and O. Reimer, Astrophys. J. **613** (2004) 962 [arXiv:astro-ph/0406254].
- [17] F. W. Stecker, S. D. Hunter and D. A. Kniffen, Astropart. Phys. **29** (2008) 25 [arXiv:0705.4311 [astro-ph]].
- [18] L. Pieri, G. Bertone and E. Branchini, Mon. Not. Roy. Astron. Soc. **384** (2008) 1627 [arXiv:0706.2101 [astro-ph]].
- [19] P. Ullio, L. Bergstrom, J. Edsjo and C. G. Lacey, Phys. Rev. D **66**, 123502 (2002) [arXiv:astro-ph/0207125].
- [20] L. Bergstrom, J. Edsjo and P. Ullio, Phys. Rev. Lett. **87**, 251301 (2001) [arXiv:astro-ph/0105048].
- [21] J. M. Siegal-Gaskins, JCAP **0810**, 040 (2008) [arXiv:0807.1328 [astro-ph]].
- [22] A. M. Green, S. Hofmann and D. J. Schwarz, Mon. Not. Roy. Astron. Soc. **353** (2004) L23 [arXiv:astro-ph/0309621].
- [23] A. M. Green, S. Hofmann and D. J. Schwarz, JCAP **0508** (2005) 003 [arXiv:astro-ph/0503387].
- [24] J. Diemand, B. Moore and J. Stadel, Nature **433** (2005) 389 [arXiv:astro-ph/0501589].
- [25] J. Diemand, M. Kuhlen and P. Madau, Astrophys. J. **649** (2006) 1 [arXiv:astro-ph/0603250].
- [26] J. F. Navarro, C. S. Frenk and S. D. M. White, Astrophys. J. **462** (1996) 563 [arXiv:astro-ph/9508025].
- [27] J. F. Navarro, C. S. Frenk and S. D. M. White, Astrophys. J. **490** (1997) 493 [arXiv:astro-ph/9611107].
- [28] J. Diemand, M. Kuhlen and P. Madau, Astrophys. J. **657** (2007) 262 [arXiv:astro-ph/0611370].
- [29] J. S. Bullock *et al.*, Mon. Not. Roy. Astron. Soc. **321** (2001) 559 [arXiv:astro-ph/9908159].
- [30] J. Diemand, M. Kuhlen, P. Madau, M. Zemp, B. Moore, D. Potter and J. Stadel, Nature **454** (2008) 735 [arXiv:0805.1244 [astro-ph]].
- [31] V. Springel *et al.*, arXiv:0809.0894 [astro-ph].
- [32] V. Springel *et al.*, arXiv:0809.0898 [astro-ph].
- [33] Einasto J., 1965, Trudy Inst. Astroz. Alma-Ata, **51**, 87
- [34] A. F. Neto *et al.*, arXiv:0706.2919 [astro-ph].
- [35] N. Fornengo, L. Pieri and S. Scopel, Phys. Rev. D **70** (2004) 103529 [arXiv:hep-ph/0407342].
- [36] W. H. Press and P. Schechter, Astrophys. J. **187** (1974) 425.
- [37] E. J. Ahn, G. Bertone and D. Merritt, Phys. Rev. D **76** (2007) 023517 [arXiv:astro-ph/0703236].
- [38] D. J. Eisenstein and W. Hu, Astrophys. J. **511** (1997) 5 [arXiv:astro-ph/9710252].
- [39] S. Ando, E. Komatsu, T. Narumoto and T. Totani, Mon. Not. Roy. Astron. Soc. **376** (2007) 1635 [arXiv:astro-ph/0610155].
- [40] <http://healpix.jpl.nasa.gov/>
- [41] K. M. Gorski, B. D. Wandelt, F. K. Hansen, E. Hivon and A. J. Banday, arXiv:astro-ph/9905275.
- [42] A. Sommerfeld, Annalen der Physik **403** (1931) 257.
- [43] S. Profumo, Phys. Rev. D **72** (2005) 103521 [arXiv:astro-ph/0508628].
- [44] M. Taoso, S. Ando, G. Bertone and S. Profumo, arXiv:0811.4493 [astro-ph].